

# A Designed Cavity in the Hydrophobic Core of a Four- $\alpha$ -Helix Bundle Improves Volatile Anesthetic Binding Affinity<sup>†</sup>

Jonas S. Johansson,<sup>\*,‡,§</sup> Brian R. Gibney,<sup>‡</sup> Francesc Rabanal,<sup>‡</sup> Konda S. Reddy,<sup>‡</sup> and P. Leslie Dutton<sup>‡</sup>

Johnson Research Foundation, Department of Biochemistry and Biophysics, and Department of Anesthesia, University of Pennsylvania, Philadelphia, Pennsylvania 19104

Received August 26, 1997; Revised Manuscript Received November 19, 1997

**ABSTRACT:** The structural features of protein binding sites for volatile anesthetics are being explored using a defined model system consisting of a four- $\alpha$ -helix bundle scaffold with a hydrophobic core. Earlier work has demonstrated that a prototype hydrophobic core is capable of binding the volatile anesthetic halothane. Exploratory work on the design of an improved affinity anesthetic binding site is presented, based upon the introduction of a simple cavity into a prototype ( $\alpha_2$ )<sub>2</sub> four- $\alpha$ -helix bundle by replacing six core leucines with smaller alanines. The presence of such a cavity increases the affinity ( $K_d = 0.71 \pm 0.04$  mM) of volatile anesthetic binding to the designed bundle core by a factor of 4.4 as compared to an analogous bundle core lacking such a cavity ( $K_d = 3.1 \pm 0.4$  mM). This suggests that such packing defects present on natural proteins are likely to be occupied by volatile general anesthetics *in vivo*. Replacing six hydrophobic core leucine residues with alanines results in a destabilization of the folded bundle by 1.7–2.7 kcal/mol alanine, although the alanine-substituted bundle still exhibits a high degree of thermodynamic stability with an overall folded conformational  $\Delta G^{\text{H}_2\text{O}} = 14.3 \pm 0.8$  kcal/mol. Covalent attachment of the spin label MTSSL to cysteine residues in the alanine-substituted four- $\alpha$ -helix bundle indicates that the di- $\alpha$ -helical peptides dimerize in an *anti* orientation. The rotational correlation time of the four- $\alpha$ -helix bundle is  $8.1 \pm 0.5$  ns, in line with earlier work on similar peptides. Fluorescence, far-UV circular dichroism, and Fourier transform infrared spectroscopies verified the hydrophobic core location of the tryptophan and cysteine residues, showing good agreement between experiment and design. These small synthetic proteins may prove useful for the study of the structural features of small molecule binding sites.

The site(s) of action of the volatile general anesthetics remain(s) unknown, despite over a century of active investigation. Extensive studies on how anesthetics might alter the physical properties of the lipid component of membranes have shown only minor effects. Current consensus therefore favors membrane proteins as the targets for volatile anesthetics (1, 2). In line with this, a number of investigators have shown that volatile anesthetics alter the function of both voltage-gated (3) and ligand-gated ion channels (4) and also ion transport proteins (5). These studies demonstrate that anesthetics are capable of altering the *activity* of a number of different membrane proteins. However, it remains to be determined whether these functional changes follow directly from anesthetic binding to the proteins in question or are an

indirect effect due to changes in the properties of membrane lipids.

In recent years, investigators have begun to directly study anesthetic binding to proteins using <sup>19</sup>F NMR spectroscopy (6–8), photoaffinity labeling (9, 10), and fluorescence spectroscopy (11–15). These studies have demonstrated that there are adventitious, but nevertheless discrete, sites present in water-soluble proteins where anesthetics may bind. Recent results for photoaffinity labeling of the *Torpedo nobiliana* nicotinic acetylcholine receptor and the sarcoplasmic reticulum Ca<sup>2+</sup>-ATPase with halothane suggest that such sites also exist in membrane proteins (10, 16).

While the above work has demonstrated the presence of binding sites for halogenated alkanes and ethers on proteins, the structural features of the binding sites remain to be defined. The feasibility of using synthetic peptides as tools to delineate the features of small molecule binding sites is being explored. As a first step toward designing an anesthetic binding site, a simple cavity (17–19) has been introduced into the hydrophobic core of a four- $\alpha$ -helix bundle scaffold, by replacing six core leucine residues with alanines. This modification increases the affinity of the anesthetic–protein interaction as compared to an analogous leucine-based core design by a factor of 4.4.

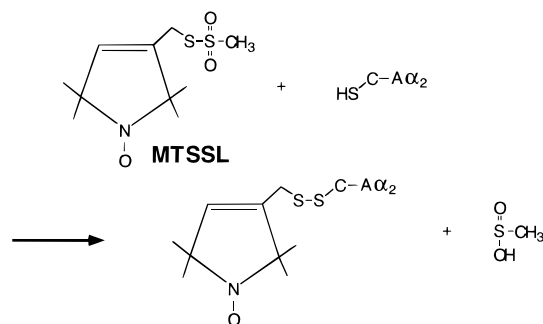
<sup>†</sup> This work was supported by NIH Grants GM27309 and GM48120 to P.L.D. and Grant GM17816 to B.R.G. J.S.J. was supported by a Foundation for Anesthesia Education and Research Young Investigator Award, a grant from the McCabe Foundation, and NIH GM55876. F.R. was supported by a grant from the European Molecular Biology Organization. The infrared spectrophotometer is supported by NIH GM48130.

\* Corresponding author mailing address: 780A Dulles, Hospital of the University of Pennsylvania, 3400 Spruce St., Philadelphia, PA 19104. Telephone: 215-349-5472. Fax: 215-349-5078. E-mail: johansso@mail.med.upenn.edu.

<sup>‡</sup> Johnson Research Foundation.

<sup>§</sup> Department of Anesthesia.

Scheme 1



## MATERIALS AND METHODS

**Materials.** Fmoc-protected amino acid perfluorophenyl esters were from PerSeptive Biosystems (Framingham, MA) with the exception of Fmoc-L-Arg(Pmc)-OPfp,<sup>1</sup> which was obtained from Bachem (King of Prussia, PA). Halothane (2-bromo-2-chloro-1,1,1-trifluoroethane) was purchased from Halocarbon Laboratories (Hackensack, NJ). The thymol preservative in the commercial halothane was removed with an aluminum oxide column (20). L-Tryptophan was from Sigma Chemical Co (St. Louis, MO). Guanidinium chloride (8.0 M) was obtained from Pierce (Rockford, IL). Hexane and 2,2,2-trifluoroethanol (NMR grade) were from Aldrich Chemical Co (Milwaukee, WI). The nitroxide spin label (1-oxyl-2,2,5,5-tetramethylpyrroline-3-methyl)methanethiosulfonate was purchased from Reanal (Budapest, Hungary). All other chemicals were reagent grade.

**Peptide Synthesis and Preparation.** Peptides were synthesized on NovaSyn PR-500 resin (Novabiochem, La Jolla, CA), using automated solid-phase technology on a Milligen 9050 (Cambridge, MA) instrument (21–25) using the Fmoc/<sup>t</sup>Bu protection strategy. Crude peptides were purified to homogeneity by reversed-phase C<sub>18</sub> HPLC (Beckman System Gold, Fullerton, CA) using aqueous acetonitrile gradients containing 0.1% (vol:vol) trifluoroacetic acid. Peptide identities were confirmed with laser desorption mass spectrometry.

Solution molecular weights for the peptides were determined on a Beckman System Gold HPLC system with a diode array detector, using a Supelco Sigmachrom GFC-100 column (300 × 7.5 mm). The elution buffer was 130 mM NaCl/20 mM sodium phosphate, pH 7.0. Molecular weight standards consisted of aprotinin (6.5 kDa), horse heart cytochrome *c* (12.4 kDa), chymotrypsinogen A (25.0 kDa), ovalbumin (43.0 kDa), and bovine serum albumin (67.0 kDa).

**Attachment of the Spin Label MTSSL.** The cysteine-specific spin label (1-oxyl-2,2,5,5-tetramethylpyrroline-3-methyl)methanethiosulfonate (MTSSL) was covalently attached to the di- $\alpha$ -helical peptide  $\alpha_2$  (Scheme 1) in a 4:1 (vol:vol) solution of 130 mM NaCl/20 mM sodium phosphate

buffer, pH 7.2, and acetonitrile, containing 1.1 mM  $\alpha_2$  with a 10-fold excess of spin label at room temperature with constant stirring for 12 h (26, 27). A single reaction product was obtained as revealed by analytical reversed-phase HPLC and laser desorption mass spectrometry. The reaction went to >99% completion as reported by HPLC. Spin-labeled peptide was in turn purified to homogeneity by reversed-phase HPLC.

**Electron Spin Resonance Spectroscopy.** Spectra were recorded at 9.479 GHz with a Bruker ESP 300E spectrometer (Billerica, MA) at room temperature, using approximately 5- $\mu$ L samples in cylindrical (0.8 mm internal diameter) Pyrex capillary tubes, placed in a 4 mm internal diameter quartz tube. The X-band frequency was measured using a Hewlett-Packard (Wilmington, DE) 5350B counter. The ESR parameters were as follows: microwave power, 10.1 mW; modulation frequency, 100 kHz; modulation amplitude, 0.993 G; time constant, 164 ms.

Curve fitting of motionally restricted nitroxides was carried out using the programs of Schneider and Freed (28) on a Microsoft Fortran Workstation. The spectral parameters for MTSSL used in the simulations were  $g_{xx} = g_{yy} = 2.0086$ ,  $g_{zz} = 2.0032$ ,  $A_{xx} = A_{yy} = 6.23$  G, and  $A_{zz} = 35.7$  G (29). The truncation parameters were  $L_{\max}^c = 14$ ,  $L_{\max}^o = 13$ ,  $K_{\max} = 10$ ,  $M_{\max} = 2$ , and  $p^1 = 2$ . The number of Lanczos steps was 50.

**Circular Dichroism Spectroscopy.** Spectra were recorded with a Model 62 DS spectropolarimeter (Aviv, Lakewood, NJ), using 1 mm (for far-UV) or 5 mm (for near-UV) path length quartz cells sealed with Teflon stoppers. The cell holder was temperature controlled at  $25.0 \pm 0.1$  °C. The buffer for the far-UV CD spectra was 10 mM potassium phosphate at pH 7.0. The bandwidth was 1.00 nm, with a scan step of 0.5 nm and an average scan time of 3.0 s for the far-UV spectra. Near-UV CD spectra were recorded with a scan time of 10.0 s and a scan step of 0.1 nm.

**Denaturation Studies.** Denaturation of four- $\alpha$ -helix bundles was followed using circular dichroism spectroscopy, monitoring the ellipticity at 222 nm ( $\Theta_{222}$ ). The measured  $\Theta_{222}$  as a function of the added denaturant concentration was fit to the equation of Mok et al. (30) describing the unfolding of a dimer (four- $\alpha$ -helix bundle) into two monomers, using a nonlinear least squares routine:

$$\text{fraction folded} = 1 - \left[ \frac{\exp(\Delta G^{\text{H}_2\text{O}} + m[\text{denaturant}])/RT}{4P(1 + (8P/(\exp(\Delta G^{\text{H}_2\text{O}} + m[\text{denaturant}])/RT)) - 1)^{1/2}} \right] \quad (1)$$

where  $\Delta G^{\text{H}_2\text{O}}$  is the conformational stability of the protein,  $m$  is the slope of the unfolding transition,  $[\text{denaturant}]$  is the molar concentration of GndCl,  $R$  is the gas constant,  $T$  is the absolute temperature, and  $P$  is the molar monomer concentration of the protein.

**Steady-State Fluorescence Measurements.** The interaction of halothane with the current four- $\alpha$ -helix bundles was followed with steady-state intrinsic tryptophan fluorescence measurements (11, 13) on a fluorescence spectrophotometer F-4500 (Hitachi, Danbury, CT). Tryptophan was excited at 295 nm, and emission spectra were recorded with peaks at 327 nm for ( $\alpha_2$ )<sub>2</sub> and 324 nm for (L $\alpha_2$ )<sub>2</sub>. The quartz cell had a path length of 10 mm and a Teflon stopper. The cell

<sup>1</sup> Abbreviations: MTSSL, (1-oxyl-2,2,5,5-tetramethylpyrroline-3-methyl)methanethiosulfonate; ( $\alpha_2$ ), helix-loop-helix peptide;  $\alpha_2$ -MTSSL, helix-loop-helix peptide with attached spin label; FTIR, Fourier transform infrared; CD, circular dichroism;  $\Theta_{222}$ , molar ellipticity at 222 nm; ESR, electron spin resonance;  $\tau_c$ , rotational correlation time; TFE, 2,2,2-trifluoroethanol; GndCl, guanidinium chloride; Fmoc, 9-fluorenylmethoxycarbonyl; <sup>t</sup>Bu, *tert*-butyl; HPLC, high-performance liquid chromatography; Pmc, 2,2,5,7,8-pentamethylchroman-6-sulfonyl; Opfp, pentafluorophenyl ester; Ac, acetyl.

holder was thermostatically controlled at  $25.0 \pm 0.1$  °C. Excitation and emission slit widths were both 5 nm. The buffer used for the fluorescence experimentation was 130 mM NaCl/20 mM sodium phosphate, pH 7.0. Protein concentration was determined with a UV/Vis Spectrometer Lambda 2 (Perkin-Elmer, Norwalk, CT), taking  $\epsilon_{280}$  for tryptophan =  $5700 \text{ M}^{-1} \text{ cm}^{-1}$  (21). Halothane-equilibrated protein, in gastight Hamilton syringes, was diluted with predetermined volumes of plain protein (treated in the same manner) to achieve the final anesthetic concentrations indicated in Figures 9 and 10.

Defining  $F_0$  as the fluorescence in the absence of halothane and  $F$  as the fluorescence in the presence of anesthetic, then

$$F = F_0 - Q \quad (2)$$

where  $Q$  is the quenched fluorescence. As described previously (11, 13), the quenched fluorescence is a function of the maximum possible quenching at an infinite halothane concentration ( $Q_{\text{max}}$ ) and the affinity of halothane for its binding site ( $K_d$ ) in the vicinity of the tryptophan residues. Assuming that no fluorescence polarization changes occur upon binding of halothane, then from mass law considerations, it follows that

$$Q = (Q_{\text{max}}[\text{halothane}])/(K_d + [\text{halothane}]) \quad (3)$$

**Fluorescence Lifetime Data Acquisition and Analysis.** Fluorescence decay kinetics were measured on a K2 multi-frequency cross-correlation phase and modulation spectrofluorometer (ISS Inc., Champaign, IL). Solutions of  $(\text{A}\alpha_2)_2$  in Teflon-stoppered 5-mm path length quartz cells, with varying concentrations of halothane, were excited at 290 nm with a 4-nm bandwidth, at room temperature. Emitted photons passed through a 308-nm cuton filter, followed by a polarizer set at the magic angle ( $55^\circ$ ) to the vertical to minimize the effect of rotational diffusion. A glycogen solution served as the scattered excitation light reference. Fluorescence lifetime data were obtained and analyzed at 20 modulation frequencies (1–300 MHz) using  $0.2^\circ$  and  $0.004^\circ$  standard error limits for phase and modulation, respectively. ISS software was used for both the acquisition (ISSL) and analysis (ISS187) of the fluorescence decay data. The fluorescence decay intensity at time  $t$ ,  $I(t)$ , was analyzed as a sum of exponentials:  $I(t) = \sum_i \alpha_i \exp(-t/\tau_i)$ , where  $\tau_i$  is the lifetime and  $\alpha_i$  is the fractional intensity of the  $i$ th decay component (31, 32). Global  $\chi^2$  minimization was used as a criteria for the goodness-of-fit of the applied model to the experimental values. A reduced  $\chi^2$  value less than 1.7 was regarded as an acceptable description of the data (33, 34). The fluorescence lifetime standard  $p$ -terphenyl in aerated ethanol was used to evaluate instrument performance, yielding a  $\tau = 1.05 \pm 0.03$  ns ( $n = 3$ ), in good agreement with the accepted value (31).

**Fourier Transform Infrared (FTIR) Spectroscopy.** FTIR spectroscopy was performed on a Bruker IFS66 instrument (Billerica, MA) using  $\text{CaF}_2$  windows and a 100- $\mu\text{m}$  path length cell. Spectra were obtained at room temperature, at intervals of  $0.5 \text{ cm}^{-1}$  with a resolution of  $2 \text{ cm}^{-1}$  over the 400–8000  $\text{cm}^{-1}$  wavenumber range. A global source was used along with a KBr beam splitter and a mercury–

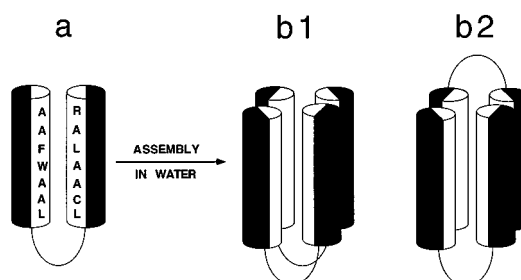


FIGURE 1: Modeled structure of four- $\alpha$ -helix bundle protein  $(\text{A}\alpha_2)_2$ . The cylinders represent the two 27-residue  $\alpha$ -helical portions of each 62-residue di- $\alpha$ -helical peptide, which are joined by an eight-residue glycine linker. Black and white halves of each cylinder represent hydrophilic and hydrophobic residues, respectively. The hydrophobic residues that occupy the **a** and **d** positions of the heptad repeat are shown in panel a, using the standard abbreviations. The 62-residue di- $\alpha$ -helical peptides (a) dimerize in water to form a four- $\alpha$ -helix bundle protein, which may have a *syn* (b1) or *anti* (b2) topology.

cadmium–telluride detector. The data were averaged after 512 successive scans.

**Gas Chromatography.** Buffer concentrations of halothane were determined using gas chromatography on an HP 6890 Series instrument (Hewlett-Packard, Wilmington, DE) as previously described (13).

**Curve Fitting and Statistics.** Best-fit curves were generated using the KaleidaGraph (Synergy Software, Reading) program. Data are expressed as mean  $\pm$  SD. Data points are the averages of at least three experiments with separate samples.

## RESULTS

**Protein Design.** The overall four- $\alpha$ -helix bundle scaffold (Figure 1) was designed to be water-soluble and to have a hydrophobic core as previously described (21–25). The four- $\alpha$ -helix-bundles used in the present study were based on prior designs (23–25) and were built from two 62-residue di- $\alpha$ -helical peptides (Figure 1), each composed of two 27-residue  $\alpha$ -helical segments and an eight-residue flexible glycine linker. The bundle designs described here have two tryptophans and two cysteines at heptad **a** positions (Figure 2a,b). The primary sequences of the two 62-residue di- $\alpha$ -helical peptides used in the current study are given in Figure 2a. The peptides described are designated  $\text{L}\alpha_2$ , with a predominantly leucine-containing core, and  $\text{A}\alpha_2$ , which has three alanines inserted at the hydrophobic **a** or **d** positions L19A, L44A, and L48A (Figure 2a,b).

As an initial approach to understanding the structural requirements of volatile anesthetic binding sites in proteins, we have designed a cavity into the hydrophobic core by replacing three leucines with alanines at **a** and **d** positions. Alanine was selected based on its smaller size and also because its intrinsic helix-forming propensity is comparable to that of leucine (35, 36). Computer modeling using Sybyl software (Tripos Associates, St. Louis, MO) on a Silicon Graphics Indigo<sup>2</sup> workstation suggested that these changes would create a cavity large enough to accommodate a halothane molecule (calculated van der Waals volume =  $123 \text{ \AA}^3$ ; 37). A tryptophan occupies an **a** position at one end of the cavity (W15, Figure 3) to permit protein concentration determination (21) and to allow anesthetic binding to be monitored (11, 13, 15). A cysteine (C41) was placed at the

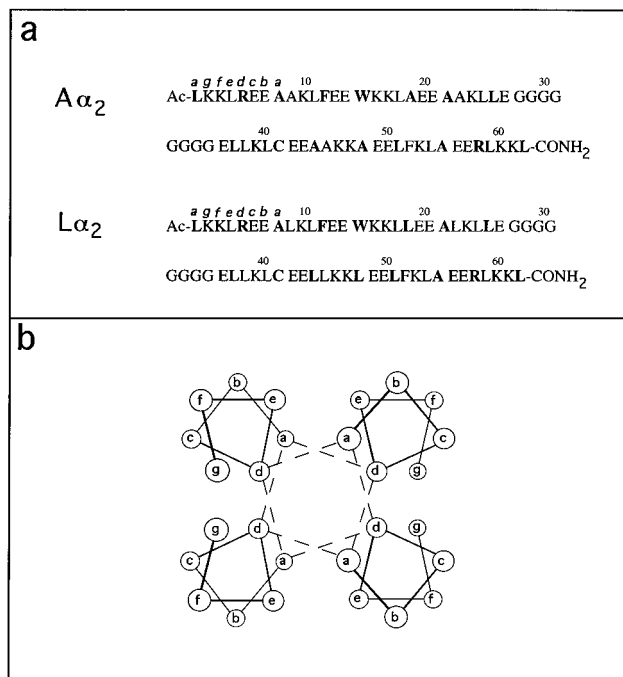


FIGURE 2: (a) Sequences of the  $A\alpha_2$  and  $L\alpha_2$  di- $\alpha$ -helical peptides with hydrophobic **a** and **d** residues shown in bold. The N-termini of the peptides are acetylated (Ac), while the C-termini have carboxamide groups. The heptad repeat assignments—*abcdefg*—used to design amphiphilic  $\alpha$ -helices are shown above the first several amino acids of each di- $\alpha$ -helical peptide. (b) End-on view of *anti* four- $\alpha$ -helical bundle showing the interaction of hydrophobic core residues at the **a** and **d** positions. The dashed lines show how successive hydrophobic core layers are composed of two **a** and two **d** residues. Modified from Betz et al. (38).

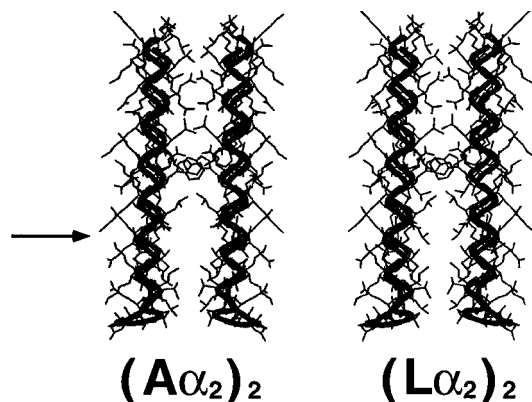


FIGURE 3: Working models of  $(A\alpha_2)_2$  and  $(L\alpha_2)_2$  created using Sybyl (Tripos Associates, St. Louis, MO) on a Silicon Graphics Indigo<sup>2</sup> workstation. The designed cavity in the hydrophobic core of  $(A\alpha_2)_2$  is shown in the lower half of the structure (indicated by the arrow). Leucine side chains are present in the corresponding region of  $(L\alpha_2)_2$ . The two tryptophan residues (W15) are located in hydrophobic positions at the midpoint in each structure.

other end of the cavity to allow (i) spin label incorporation and (ii) the environment of the thiol group to be probed by infrared spectroscopy.

**Overall Topology of the Four- $\alpha$ -Helix Bundle ( $A\alpha_2$ )<sub>2</sub>.** Earlier studies have shown that the orientation of different di- $\alpha$ -helical peptides that dimerize to form four- $\alpha$ -helix bundles may be either *syn* (22, 38) or *anti* (24, 39). The topology of the di- $\alpha$ -helical peptides in the four- $\alpha$ -helix bundle  $(A\alpha_2)_2$  was investigated by attaching the spin label MTSSL to C41. A *syn* bundle orientation (Figure 1b1) was

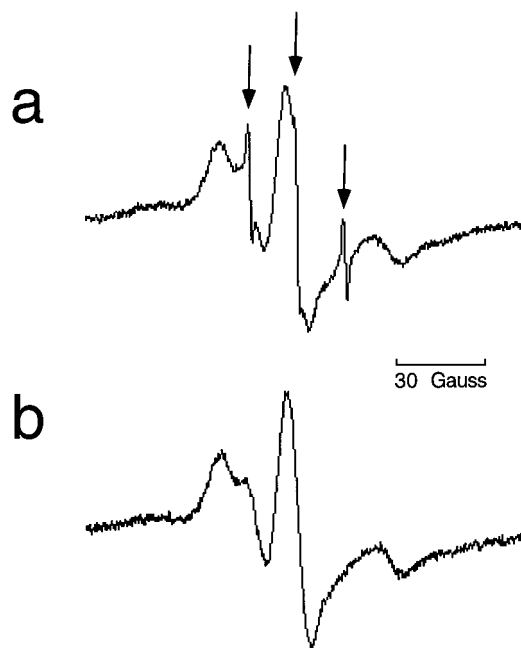


FIGURE 4: Room temperature ESR spectra of  $(A\alpha_2\text{-MTSSL})_2$  in the (a) absence and (b) presence of 250  $\mu\text{M}$  Ni(II). Total peptide concentration was 37  $\mu\text{M}$  for both conditions. The vertical arrows in panel a indicate the resonances of the more rapidly tumbling nitroxide fraction.

predicted to yield an ESR spectrum consisting of equal contributions from both mobile and confined spin labels. This results from steric crowding in the hydrophobic core, which forces one of the nitroxides out into the solvent (24). Alternatively, an *anti* bundle orientation (Figure 1b2) allows both spin labels to be located in the hydrophobic core, yielding a one-component broadened ESR spectrum (24).

Figure 4a shows the ESR spectrum for MTSSL bound to  $(A\alpha_2)_2$ . The shape of the spectrum is characteristic of a predominantly motionally restricted spin label, with a superimposed minor more rapidly tumbling nitroxide fraction (vertical arrows). Adding the water-soluble paramagnetic relaxation agent nickel(II)—as  $\text{NiCl}_2$ —eliminates the contribution from the rapidly tumbling component (Figure 4b). Spectral integration revealed that less than 1% of the total ESR signal is accessible to nickel(II), indicating that one of the two MTSSL spin labels in a minority of the  $(A\alpha_2)_2$  bundles is solvent exposed and therefore undergoes paramagnetic relaxation. This suggests that the topology of the majority (>99%) of the bundles is *anti* as shown in Figure 1b2, allowing both spin labels (per four- $\alpha$ -helix bundle) to be accommodated within the hydrophobic core. *Anti* dimerization is thus favored by approximately 2.7 kcal/mol bundle over the *syn* orientation.

Analysis of the line widths in Figure 4b by spectral simulation (see Figure 11a) yielded a rotational correlation time ( $\tau_c$ ) of  $8.1 \pm 0.5$  ns, corresponding to the predicted rotational correlation time of the bundle as a whole (24). This suggests that there is little, or no, motional freedom of the confined MTSSL label in the hydrophobic core, independent of the overall tumbling of the four- $\alpha$ -helix bundle.

**Conformational Stabilities of the Four- $\alpha$ -Helix Bundles ( $A\alpha_2$ )<sub>2</sub> and ( $L\alpha_2$ )<sub>2</sub>.** The effect of decreased hydrophobic core packing on four- $\alpha$ -helix bundle stability was assessed with guanidinium chloride denaturation of  $(A\alpha_2)_2$ ,  $(A\alpha_2\text{-MTSSL})_2$ ,

Table 1: Spectral and Thermodynamic Properties of the Four- $\alpha$ -Helix Bundles ( $A\alpha_2$ )<sub>2</sub>, ( $A\alpha_2$ -MTSSL)<sub>2</sub>, and ( $L\alpha_2$ )<sub>2</sub>

four-helix bundle	solution MWt (kDa)	fluorescence maximum (nm)	$\Delta G^{H_2O}$ (kcal/mol)	$m$ (kcal/mol·M)	$[\Theta]_{222}$ (deg cm <sup>2</sup> dmol <sup>-1</sup> )	halothane $K_d$ (mM)
( $A\alpha_2$ ) <sub>2</sub>	20.3	327	14.3 $\pm$ 0.8	2.0 $\pm$ 0.2	23 000 <sup>a</sup>	0.71 $\pm$ 0.04
( $A\alpha_2$ -MTSSL) <sub>2</sub>			15.3 $\pm$ 0.5 <sup>b</sup>	1.9 $\pm$ 0.1 <sup>b</sup>	25 800 <sup>a</sup>	
			15.9 $\pm$ 0.8 <sup>c</sup>	1.9 $\pm$ 0.2 <sup>c</sup>		
( $L\alpha_2$ ) <sub>2</sub>	20.5	324	>30		24 400 <sup>a</sup>	3.1 $\pm$ 0.4

<sup>a</sup> Calculated as described in Robertson et al. (21). <sup>b</sup> Determined using CD spectroscopy. <sup>c</sup> Determined using EPR spectroscopy.

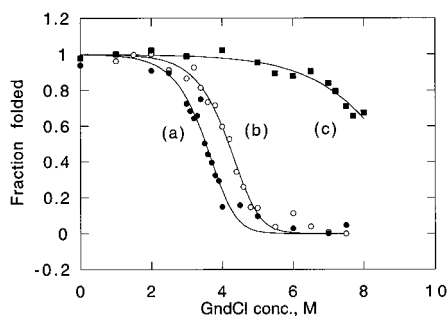


FIGURE 5: Four- $\alpha$ -helix bundle denaturation curves as monitored by spectropolarimetry at 222 nm. (a) ( $A\alpha_2$ )<sub>2</sub>, (b) ( $A\alpha_2$ -MTSSL)<sub>2</sub>, and (c) ( $L\alpha_2$ )<sub>2</sub>. The calculated  $\Delta G^{H_2O}$  and  $m$  values using eq 1 are given in Table 1.

and ( $L\alpha_2$ )<sub>2</sub>. The ellipticity at 222 nm for the four- $\alpha$ -helix bundles was measured as a function of the added denaturant concentration, and the data were fitted using eq 1. Figure 5a,b shows that both ( $A\alpha_2$ )<sub>2</sub> and ( $A\alpha_2$ -MTSSL)<sub>2</sub> undergo complete denaturation, whereas ( $L\alpha_2$ )<sub>2</sub> shows only a partial denaturation transition (Figure 5c). This suggests that the hydrophobic core of ( $L\alpha_2$ )<sub>2</sub> is presumably better packed than that of ( $A\alpha_2$ )<sub>2</sub>. Calculated  $\Delta G^{H_2O}$  and  $m$  values for ( $A\alpha_2$ )<sub>2</sub> and ( $L\alpha_2$ )<sub>2</sub> are given in Table 1. The covalent attachment of MTSSL to ( $A\alpha_2$ )<sub>2</sub> results in an increase in the overall stability of the four- $\alpha$ -helix bundle (Figure 5b and Table 1), consistent with the location of the spin label in the hydrophobic core, at sites otherwise characterized by core packing defects.

The ESR spectrum for ( $A\alpha_2$ -MTSSL)<sub>2</sub> reveals that GndCl leads to an increase in the peak height and a narrowing of the resonances as the bundle denatures (not shown). The calculated thermodynamic parameters for bundle stability based on ESR spectral analysis are  $\Delta G^{H_2O} = 15.9 \pm 0.8$  kcal/mol and  $m = 1.9 \pm 0.2$  kcal/mol·M, values comparable to those obtained with CD measurements (Table 1). This indicates that both secondary and tertiary structural features are denatured simultaneously in this bundle system.

*Verifying the Hydrophobic Core Location of Residues W15 and C41 in ( $A\alpha_2$ )<sub>2</sub>.* The ( $A\alpha_2$ )<sub>2</sub> bundle contains two tryptophan residues that display a single fluorescence emission maximum at 327 nm (see Figure 8), indicating that both indole rings are well protected from the surrounding aqueous solvent and are located in the hydrophobic core as designed. The near-UV CD spectrum (Figure 6a) shows that the two tryptophan residues are responsible for a well-resolved CD signal, with two positive bands centered at 280 and 288 nm, suggesting that the indole rings are motionally constrained in the hydrophobic core (40, 41). In addition, there is a positive near-UV CD band with a maximum amplitude at 257 nm, which is attributed, in part, to the four phenylalanines present in each bundle. The addition of 8 M GndCl results in complete loss of the near-UV CD signal, consistent

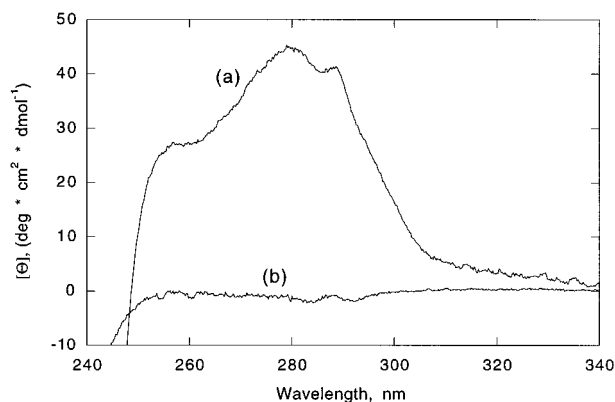


FIGURE 6: (a) Near-UV CD spectra for the ( $A\alpha_2$ )<sub>2</sub> bundle showing the contribution of W15. The peptide concentration was 0.49 mM in 130 mM NaCl/20 mM sodium phosphate buffer, pH 7.0. The ellipticity of the sample was recorded every 0.1 nm, with a 10-s averaging time. (b) Near-UV CD spectrum for 0.48 mM ( $A\alpha_2$ )<sub>2</sub> in 8 M GndCl.

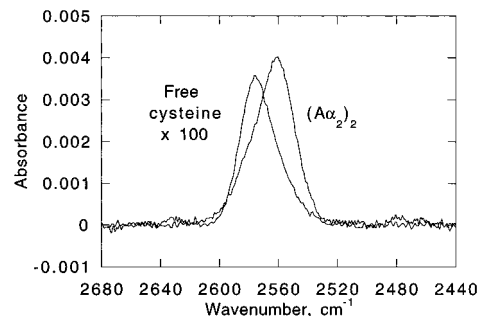


FIGURE 7: Infrared S-H stretch spectrum for C41 in the four- $\alpha$ -helix bundle ( $A\alpha_2$ )<sub>2</sub> at pH 7.1. Peptide concentration was 5 mM. The frequency of absorption = 2561 cm<sup>-1</sup>. For comparison, the S-H stretch for free cysteine (500 mM) at pH 7.1 is shown magnified 100-fold.

with the tryptophan and phenylalanine residues becoming free to assume additional conformations (Figure 6b).

The environment of the cysteine at position 41 (C41) was examined by FTIR spectroscopy. Figure 7 shows that the S-H stretch vibrations of the two thiol groups per four- $\alpha$ -helix bundle have a relatively intense absorption band centered on 2561 cm<sup>-1</sup> ( $\epsilon = 0.08$  mM<sup>-1</sup> cm<sup>-1</sup>). This indicates that the cysteines are well shielded from the solvent (42, 43) and located in the hydrophobic core as designed. For comparison, the thiol stretch of *free* cysteine at pH 7.1 is shown, with a band centered on 2576 cm<sup>-1</sup> and an extinction coefficient that is approximately 100-fold less than that displayed by the C41 residue. The frequency of the C41 S-H vibration in ( $A\alpha_2$ )<sub>2</sub> suggests that the thiol groups are forming hydrogen bonds with neighboring groups, probably backbone carbonyl oxygens, or perhaps with structured water molecules located in the hydrophobic core packing defect (42, 43).

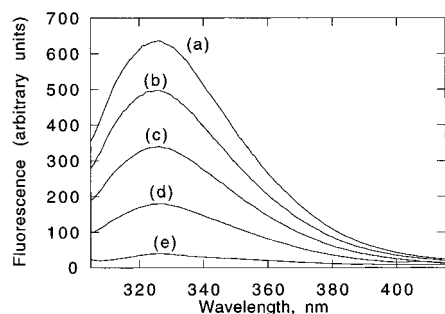


FIGURE 8: Halothane concentration-dependent quenching of the  $(A\alpha_2)_2$  four- $\alpha$ -helix bundle ( $5 \mu\text{M}$ ) fluorescence. Excitation was at 295 nm, with the emission maximum at 327 nm. The concentrations of halothane were (a) 0, (b) 0.18, (c) 0.70, (d) 1.8, and (e) 5.3 mM.

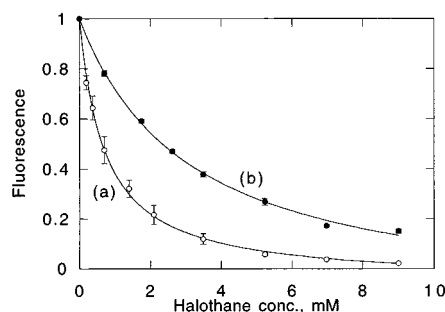


FIGURE 9: Comparison of quenching profiles for (a)  $(A\alpha_2)_2$  and (b)  $(L\alpha_2)_2$  tryptophan fluorescence by halothane. Bundle protein concentration was  $5 \mu\text{M}$  in both cases. The data points are the means of three to six experiments on separate samples, with the error bars representing the SD. The line through the data points has the form of eq 3.

The spectroscopic analyses described above suggest that the designed hydrophobic core anesthetic binding sites are contained within an *anti* scaffold as modeled in Figure 1b2 and that both W15 and C41 are in the hydrophobic core. This implies that there will be two identical potential binding sites in each four- $\alpha$ -helix bundle core. Other residues lining the designed binding site include leucines, alanines, phenylalanine, and arginine (Figure 1a).

**Binding of the Volatile Anesthetic Halothane to the Core of the Four- $\alpha$ -Helix Bundles  $(A\alpha_2)_2$  and  $(L\alpha_2)_2$ .** The binding of halothane to the designed sites in the four- $\alpha$ -helix-bundle  $(A\alpha_2)_2$  hydrophobic core was followed by tryptophan fluorescence quenching (11, 13, 15) as shown in Figure 8. Halothane causes a concentration-dependent quenching of the fluorescence without changing the emission maximum, indicating that halothane binding is not accompanied by changes in the dielectric environment local to the indole rings. Lack of a red-shift in the tryptophan fluorescence emission maximum upon halothane binding suggests that the anesthetic does not promote unfolding of the bundle, which leads to any increased water exposure of the indole rings. Figure 9a shows a plot of the  $(A\alpha_2)_2$  bundle tryptophan fluorescence as a function of the halothane concentration. Fitting the data using eq 3 yields a  $K_d = 0.71 \pm 0.04$  mM with a  $Q_{\max} = 1.06 \pm 0.02$ , indicating that the fluorescence of both of the tryptophan residues in the bundle core is quenched by bound anesthetic. For comparison, Figure 9b shows the measured binding of halothane to the better packed  $(L\alpha_2)_2$  bundle core. The calculated binding parameters using eq 3 are  $K_d = 3.1 \pm 0.4$  mM and  $Q_{\max} = 1.02 \pm 0.06$ , again

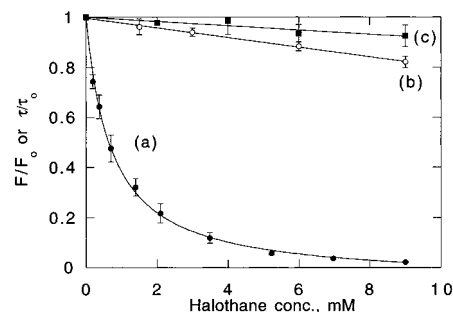


FIGURE 10: (a) Quenching of  $(A\alpha_2)_2$  ( $5 \mu\text{M}$ ) tryptophan fluorescence as a function of halothane concentration. The data points are the means of three to six experiments on separate samples, with the error bars representing the SD. The line through the data points has the form of eq 3. (b) Effect of halothane on  $A\alpha_2$  tryptophan fluorescence in the presence of 50% TFE. Data points are the means of three experiments with error bars representing the SD. (c) Effect of halothane on the long-lived component of the tryptophan fluorescence lifetime of  $(A\alpha_2)_2$ . The concentration of  $(A\alpha_2)_2$  was  $18 \mu\text{M}$ . Data points are the means of three experiments with error bars representing the SD.

implying that the fluorescence of both tryptophan residues is quenched. The affinity of halothane binding to the more tightly packed core in  $(L\alpha_2)_2$  is however decreased as compared to the  $(A\alpha_2)_2$  bundle by a factor of 4.4.

The importance of bundle tertiary structural interactions for anesthetic binding is shown in Figure 10b, which demonstrates the diminished quenching of tryptophan fluorescence by halothane after bundle dissociation with trifluoroethanol. Trifluoroethanol negates the hydrophobic interactions that underlie four- $\alpha$ -helix bundle formation (44) while maintaining secondary structure (45). The magnitude of fluorescence quenching in 50% TFE is comparable to that measured when halothane is added to *free* L-tryptophan in solution (11, 13) and results from collisional encounters between halothane and the dissociated di- $\alpha$ -helix peptides.

Fluorescence lifetime analysis was used to differentiate between static and dynamic quenching (46) for  $(A\alpha_2)_2$  bundle tryptophan fluorescence quenching by halothane. A static interaction follows association between fluorophore and quencher, as might be expected with a ligand-protein interaction involving the fluorophore. Global  $\chi^2$  minimization was achieved using biexponential fits with lifetimes of  $0.7 \pm 0.1$  and  $4.0 \pm 0.1$  ns for  $(A\alpha_2)_2$ . The pre-exponential factor was 1:9 for the short- and long-lived components, respectively. Assignment of lifetimes in the presence of halothane revealed that the longer lifetime component decreased by only  $7 \pm 3\%$  in the presence of 9 mM halothane (Figure 9c). Thus, the fluorescence changes measured under steady-state conditions (Figure 9a) far exceed those that can be attributed solely to collisional quenching (Figure 9c). This result indicates that a static mechanism is principally responsible for the observed steady-state fluorescence quenching, strongly implying that halothane indeed binds to the hydrophobic core of  $(A\alpha_2)_2$  in the vicinity of the tryptophan residues.

Further evidence for bundle dissociation by trifluoroethanol is given by the MTSSL spectra in Figure 11. In Figure 11a, the ESR spectrum for the MTSSL label confined in the hydrophobic core of the bundle is shown with a  $\tau_c = 8.1 \pm 0.5$  ns. This is comparable to the  $\tau_c = 7.3 \pm 0.5$  ns reported for a similar four- $\alpha$ -helix bundle with a maleimide spin label

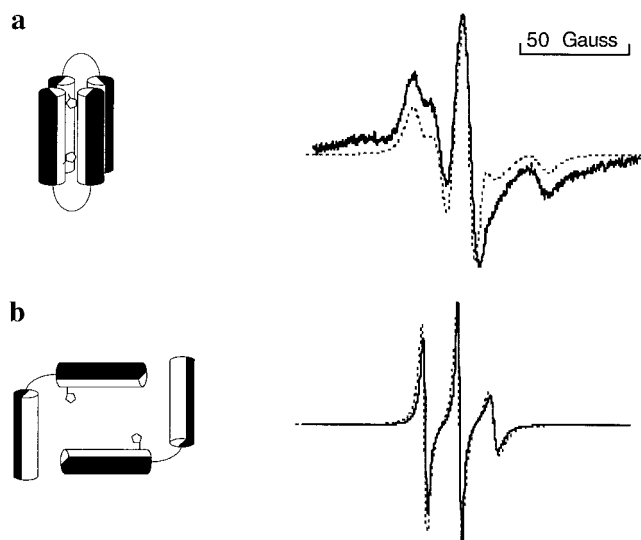


FIGURE 11: ESR spectra for  $(A\alpha_2\text{-MTSSL})_2$  in the absence (a) and presence (b) of 50% (6.9 M) trifluoroethanol. The intensity of the resonances in panel b have been decreased by a factor of 20. Simulated spectra are shown as dotted lines. Cartoons to the left illustrate peptide configurations that are compatible with the ESR spectra.

incorporated into the core (24). Adding 50% TFE results in the ESR spectrum shown in Figure 11b, with a  $\tau_c = 1.1 \pm 0.3$  ns, as the mobility of the spin label is enhanced following bundle dissociation to form di- $\alpha$ -helical peptides. Again, this agrees well with prior work using a spin-labeled four- $\alpha$ -helix bundle of similar size, which reported a  $\tau_c = 2.5 \pm 0.5$  ns in the presence of 40% TFE (24). The somewhat increased  $\tau_c$  measured in the earlier work is attributed to the lower denaturant concentration used.

## DISCUSSION

There is at present very little known about the structural features of volatile anesthetic binding sites on protein targets. This follows from (i) the relatively low affinity of the interactions, which display dissociation constants in the millimolar range; (ii) the structural complexity of the membrane proteins that are currently considered to be the targets for anesthetic action; and (iii) the lack of information about how anesthetics interact with proteins. The procedure adopted in the present paper using the four- $\alpha$ -helix bundle motif, which serves as a scaled down model of the lipid bilayer spanning portions of the large membrane proteins, is aimed at a molecular level understanding of anesthetic-protein complexation. The advantages of using the synthetic four- $\alpha$ -helix bundle scaffolds to study anesthetic-protein interactions are that they are (i) structurally defined; (ii) readily amenable to modification using protein engineering; and (iii) far less complex than natural membrane proteins, allowing for precise structural and dynamic descriptions of the ligand-protein complexes.

In general, binding of a ligand by a protein depends on (i) the presence of a cavity, groove, or cleft, allowing for steric complementarity such that no van der Waals overlap occurs while simultaneously minimizing the residual free space between interacting atoms; (ii) electrostatic complementarity, which pairs unlike partial and formal charges; and (iii) the hydrophobic effect (47, 48). The volatile anesthetic binding site described here was designed by simple replace-

ment of leucines in  $(L\alpha_2)_2$  by alanines to create  $(A\alpha_2)_2$ , thereby maintaining the hydrophobic nature of the bundle interior but creating sites to accommodate halothane. The sites have an improved affinity for the anesthetic as compared to the bundle  $(L\alpha_2)_2$ . In addition, the binding sites in  $(A\alpha_2)_2$  have an improved affinity for halothane as compared to a prototype bundle scaffold designed to bind hemes (21, 22), with a histidine and leucine core (13). The binding domain in  $(A\alpha_2)_2$  is lined by aliphatic leucine and alanine residues and by tryptophan, cysteine, phenylalanine, and arginine. The improved affinity is consistent with the creation of a binding pocket resulting from the replacement of larger leucine residues (van der Waals volume  $124 \text{ \AA}^3$ ; 49) by smaller alanines ( $67 \text{ \AA}^3$ ). Assuming that there is no structural rearrangement associated with the leucine to alanine substitutions, the cavity size has an upper estimate of  $171 \text{ \AA}^3$ . For comparison, halothane has a calculated van der Waals volume of  $123 \text{ \AA}^3$ .

In addition to van der Waals interactions, there exists the potential for weak hydrogen bond formation between the halothane hydrogen atom and either the indole ring  $\pi$ -electrons, which can act as a hydrogen bond acceptor (50, 51), or the electronegative cysteine sulfur atom (52). Halothane has the potential to act as a hydrogen bond acceptor via one or more of its halogen atoms (53–55), which may interact favorably with either indole ring hydrogens or with the cysteine sulfhydryl group. While the detailed structure of the complex formed between halothane and  $(A\alpha_2)_2$  remains to be determined, it is clear that the anesthetic resides in the vicinity of the hydrophobic core tryptophan residues as designed, since fluorescence quenching by heavy atoms is a short-range phenomenon occurring over a distance less than  $3\text{--}5 \text{ \AA}$  (56, 57).

The decreased hydrophobic core packing of  $(A\alpha_2)_2$  is reflected in its lesser overall stability ( $\Delta G^{\text{H}_2\text{O}} = 14.3$  kcal/mol), compared to the bundle  $(L\alpha_2)_2$  with a hydrophobic core composed primarily of leucine residues ( $\Delta G^{\text{H}_2\text{O}} = >30$  kcal/mol). The finding that covalent attachment of the spin label MTSSL to  $(A\alpha_2)_2$  enhances bundle stability suggests that the overall effect of the nitroxide is to improve core packing. The leucine-based bundle core  $(L\alpha_2)_2$  undergoes only a 30% chemical denaturation in the presence of 8 M guanidinium chloride at  $25^\circ\text{C}$ . Similar high stability four- $\alpha$ -helix bundles with predominantly leucine-containing hydrophobic cores have been described previously (24, 58). It is therefore not possible to calculate accurate thermodynamic parameters for  $(L\alpha_2)_2$ . However, as an approximation, we can compare the stability of  $(A\alpha_2)_2$  with a previous cysteine-containing bundle design (24). Replacing six leucines with alanines in the core is found to destabilize the folded form of the protein by 10–16 kcal/mol or approximately 1.7–2.7 kcal/mol per alanine residue. This effect on global protein stability is in good agreement with work on leucine to alanine mutants in the hydrophobic core of T4 lysozyme (59) and the natural four- $\alpha$ -helix bundle protein ROP (repressor of primer; 60). Halothane binding to the bundle cavity in  $(A\alpha_2)_2$  is therefore more favorable than in the absence of the cavity [in  $(L\alpha_2)_2$ ] because (i) of the creation of additional van der Waals interactions between anesthetic and protein; and (ii) the overall transfer free energy from water to the protein site is not compromised by the enthalpic cost of creating such a cavity for the anesthetic. Displacement of structured water

molecules from the hydrophobic core of (A $\alpha$ <sub>2</sub>)<sub>2</sub> upon halothane binding would also contribute a favorable entropic component to the overall binding energetics.

Replacing six core leucines in (L $\alpha$ <sub>2</sub>)<sub>2</sub> with alanines to form (A $\alpha$ <sub>2</sub>)<sub>2</sub> is shown to increase the affinity of halothane binding to the hydrophobic core by a factor of 4.4 ( $K_d$  values of 3.1 and 0.71 mM, respectively). The designed volatile anesthetic binding sites in (A $\alpha$ <sub>2</sub>)<sub>2</sub> have a higher affinity than the best characterized binding sites for halothane described so far, displaying about two times the average affinity ( $K_d = 1.3\text{--}1.8 \pm 0.2$  mM) of the sites in bovine serum albumin (7, 11). It is possible that the affinity of the anesthetic-protein interaction may be improved further by decreasing the cavity size, thereby further optimizing the van der Waals interactions between anesthetic and protein.

This initial effort to engineer an improved affinity binding site for a small hydrophobic molecule, with limited interaction potential, into a four- $\alpha$ -helix bundle scaffold may have relevance for the design of artificial enzymes. Noncovalent binding is the primary event in catalysis, and the results of the present study indicate that substrate binding will be favored by the presence of a pre-existing site on the protein that accommodates the substrate sterically.

Using the designed synthetic peptide approach to probe the structural features of volatile anesthetic-protein complexes, it will be possible to carry out a systematic survey of the effects of a variety of amino acid side chains on the binding energetics. This may allow predictions to be made concerning the structural composition of the *in vivo* general anesthetic target sites. Furthermore, this approach allows a test of the hypothesis that the clinical EC<sub>50</sub> for halothane of approximately 250  $\mu$ M might correspond to the  $K_d$  of a single protein target, increasing the likelihood of the existence of such "high" affinity anesthetic binding sites in the central nervous system. Finally, the structural and dynamic consequences of anesthetic binding to such designed sites contained in simplified scaffolds are amenable to detailed analysis using spectroscopic approaches, providing insight into how anesthetic complexation might alter protein function.

## ACKNOWLEDGMENT

Mass spectrometry analyses were performed by the Protein Chemistry Laboratory, University of Pennsylvania, Philadelphia, PA.

## REFERENCES

- Franks, N. P., and Lieb, W. R. (1994) *Nature* 367, 607–614.
- Harris, R. A., Mihic, S. J., Dildy-Mayfield, J. E., and Machu, T. K. (1995) *FASEB J.* 9, 1454–1462.
- Takenoshita, M., and Steinbach, J. H. (1991) *J. Neurosci.* 11, 1404–1412.
- Forman, S. A., Miller, K. W., and Yellen, G. (1995) *Mol. Pharmacol.* 48, 574–581.
- Karon, B. S., Geddis, L. M., Kutchai, H., and Thomas, D. D. (1995) *Biophys. J.* 68, 936–945.
- Dubois, B. W., and Evers, A. S. (1992) *Biochemistry* 31, 7069–7076.
- Dubois, B. W., Cherian, S. F., and Evers, A. S. (1993) *Proc. Natl. Acad. Sci. U.S.A.* 90, 6478–6482.
- Xu, Y., Tang, P., Firestone, L., and Zhang, T. T. (1996) *Biophys. J.* 70, 532–538.
- Eckenhoff, R. G., and Shuman, H. (1993) *Anesthesiology* 79, 96–106.
- Eckenhoff, R. G. (1996) *Proc. Natl. Acad. Sci. U.S.A.* 93, 2807–2810.
- Johansson, J. S., Eckenhoff, R. G., and Dutton, P. L. (1995) *Anesthesiology* 83, 316–324.
- Johansson, J. S., and Eckenhoff, R. G. (1996) *Biochim. Biophys. Acta* 1290, 63–68.
- Johansson, J. S., Rabanal, F., and Dutton, P. L. (1996) *J. Pharmacol. Exp. Ther.* 279, 56–61.
- Raines, D. E., and McClure, K. B. (1997) *Anesthesiology* 86, 476–486.
- Johansson, J. S. (1997) *J. Biol. Chem.* 272, 17961–17965.
- Kosk-Kosicka, D., Fomitcheva, I., Lopez, M. M., and Eckenhoff, R. G. (1997) *FEBS Lett.* 402, 189–192.
- Rashin, A. A., Iofin, M., and Honig, B. (1986) *Biochemistry* 25, 3619–3625.
- Hubbard, S. J., Gross, K.-H., and Argos, P. (1994) *Protein Eng.* 7, 613–626.
- Williams, M. A., Goodfellow, J. M., and Thornton, J. M. (1994) *Protein Sci.* 3, 1224–1235.
- Shibata, A., Morita, K., Yamashita, T., Kamaya, H., and Ueda, I. (1991) *J. Pharm. Sci.* 80, 1037–1041.
- Robertson, D. E., Farid, R. S., Moser, C. C., Urbauer, J. L., Mulholland, S. E., Pidikiti, R., Lear, J. D., Wand, A. J., DeGrado, W. F., and Dutton, P. L. (1994) *Nature* 368, 425–432.
- Rabanal, F., DeGrado, W. F., and Dutton, P. L. (1996) *J. Am. Chem. Soc.* 118, 473–474.
- Gibney, B. R., Mulholland, S. E., Rabanal, F., and Dutton, P. L. (1996) *Proc. Natl. Acad. Sci. U.S.A.* 93, 15041–15046.
- Gibney, B. R., Johansson, J. S., Rabanal, F., Skalicky, J. J., Wand, A. J., and Dutton, P. L. (1997) *Biochemistry* 36, 2798–2806.
- Gibney, B. R., Rabanal, F., Skalicky, J. J., Wand, A. J., and Dutton, P. L. (1997) *J. Am. Chem. Soc.* 119, 2323–2324.
- Mchaurab, H. S., Hyde, J. S., and Feix, J. B. (1993) *Biochemistry* 32, 11895–11902.
- Oh, K. J., Zhan, H., Cui, C., Hideg, K., Collier, R. J., and Hubbell, W. L. (1996) *Science* 273, 810–812.
- Schneider, D. J., and Freed, J. H. (1989) in *Biological Magnetic Resonance* (Berliner, L. J., and Reuben, J., Eds.) pp 1–76, Plenum Press, New York.
- Calciano, L. J., Escobar, W. A., Millhauser, G. L., Miick, S. M., Rubaloff, J., Todd, A. P., and Fink, A. L. (1993) *Biochemistry* 32, 5644–5649.
- Mok, Y.-K., De Prat Gay, G., Butler, P. J., and Bycroft, M. (1996) *Protein Sci.* 5, 310–319.
- Lakowicz, J. R. (1983) *Principles of Fluorescence Spectroscopy*, Plenum Press, New York.
- Beechem, J. M., and Brandt, L. (1985) *Annu. Rev. Biochem.* 54, 43–71.
- Lakowicz, J. R., Laczko, G., Cherek, H., Gratton, E., and Limkeman, M. (1984) *Biophys. J.* 46, 463–477.
- Gratton, E., Limkeman, M., Lakowicz, J. R., Maliwal, B. P., Cherek, H., and Laczko, G. (1984) *Biophys. J.* 46, 479–486.
- Padmanabhan, S., Marqusee, S., Ridgeway, T., Laue, T. M., and Baldwin, R. L. (1990) *Nature* 344, 268–270.
- Bryson, J. W., Betz, S. F., Lu, H. S., Suich, D. J., Zhou, H. X., O'Neil, K. T., and DeGrado, W. F. (1995) *Science* 270, 935–941.
- Abraham, M. H., and McGowan, J. C. (1987) *Chromatographia* 23, 243–6.
- Betz, S. F., Liebman, P. A., and DeGrado, W. F. (1997) *Biochemistry* 36, 2450–2458.
- Grosset, A. M., Rabanal, F., Farid, R. S., Robertson, D. E., Pilloud, D. L., DeGrado, W. F., and Dutton, P. L. (1996) in *Peptides: Chemistry, Structure and Biology* (Kaumaya, P. T. P., and Hodges, R. S., Eds.) pp 573–574, Mayflower Scientific Ltd., Kingswinford, U.K.
- Strickland, E. H. (1974) *CRC Crit. Rev. Biochem.* 3, 113–175.
- Handel, T. M., Williams, S. A., Menyhard, D., and DeGrado, W. F. (1993) *J. Am. Chem. Soc.* 115, 4457–4460.

42. Alben, J. O., Bare, G. H., and Bromberg, P. A. (1974) *Nature* 252, 736–738.
43. Dong, A., and Caughey, W. S. (1994) *Methods Enzymol.* 232, 139–175.
44. Zhou, N. E., Kay, C. M., and Hodges, R. S. (1992) *J. Biol. Chem.* 267, 2664–2670.
45. Jasanoff, A., and Fersht, A. R. (1994) *Biochemistry* 33, 2129–2135.
46. Eftink, M. R., and Ghiron, C. A. (1981) *Anal. Biochem.* 114, 199–227.
47. Náráy-Szabó, G. (1993) *J. Mol. Recognit.* 6, 205–210.
48. Peters, K. P., Fauck, J., and Frömmel, C. (1996) *J. Mol. Biol.* 256, 201–213.
49. Richards, F. M. (1974) *J. Mol. Biol.* 82, 1–14.
50. Burley, S. K., and Petsko, G. A. (1988) *Adv. Protein Chem.* 39, 125–189.
51. Katz, B. A., Liu, B., and Cass, R. (1996) *J. Am. Chem. Soc.* 118, 7914–7920.
52. Viguera, A. R., and Serrano, L. (1995) *Biochemistry* 34, 8771–8779.
53. Murray-Rust, P., Stallings, W. C., Monti, C. T., Preston, R. K., and Glusker, J. P. (1983) *J. Am. Chem. Soc.* 105, 3206–3214.
54. Shimoni, L., Carrell, H. L., Glusker, J. P., and Coombs, M. M. (1994) *J. Am. Chem. Soc.* 116, 8162–8168.
55. Glusker, J. P. (1995) *Acta Crystallogr. D51*, 418–427.
56. Tsao, D. H. H., Casa-Finet, J. R., Maki, A. H., and Chase, J. W. (1989) *Biophys. J.* 55, 927–936.
57. Basu, G., Anglos, D., and Kuki, A. (1993) *Biochemistry* 32, 3067–3076.
58. Munson, M., Balasubramanian, S., Fleming, K. G., Nagi, A. D., O'Brien, R., Sturtevant, J., and Regan, L. (1996) *Protein Sci.* 5, 1584–1593.
59. Eriksson, A. E., Baase, W. A., Zhang, X.-J., Heinz, D. W., Blaber, M., Baldwin, E. P., and Matthews, B. W. (1992) *Science* 255, 178–183.
60. Steif, C., Hinz, H.-J., and Cesareni, G. (1995) *Proteins* 23, 83–96.

BI9721290